


## Dissecting Mott and charge-density wave dynamics in the photoinduced phase of $1T$ -TaS<sub>2</sub>

Alberto Simoncig,<sup>1</sup> Matija Stupar,<sup>2</sup> Barbara Ressel ,<sup>2</sup> Tanusree Saha,<sup>2</sup> Primoz Rebernik Ribic,<sup>1,2</sup> and Giovanni De Ninno<sup>1,2</sup>

<sup>1</sup>*Elettra Sincrotrone Trieste S.C.p.A., Area Science Park, 34149 Basovizza (TS), Italy*

<sup>2</sup>*Laboratory of Quantum Optics, University of Nova Gorica, 5001 Nova Gorica, Slovenia*



(Received 21 October 2020; revised 5 March 2021; accepted 11 March 2021; published 12 April 2021)

The two-dimensional transition-metal dichalcogenide  $1T$ -TaS<sub>2</sub> is a complex material standing out for its puzzling low temperature phase marked by signatures amenable to both Mott-insulating and charge-density wave states. Electronic Mott states, coupled to a lattice, respond to coherent optical excitations via a modulation of the lower (valence) Hubbard band. Such dynamics is driven by strong electron-phonon coupling and typically lasts for tens of picoseconds, mimicking coherent structural distortions. Instead, the response occurring at the much faster timescale, mainly dominated by electronic many-body effects, is still a matter of intense research. By performing time- and angle-resolved photoemission spectroscopy, we investigated the photoinduced phase of  $1T$ -TaS<sub>2</sub> and found out that its lower Hubbard band promptly reacts to coherent optical excitations by shifting its binding energy towards a slightly larger value. This process lasts for a time comparable to the optical pump pulse length, mirroring a transient change of the onsite Coulomb repulsion energy ( $U$ ). Such an observation suggests that the correction to the bare value of  $U$ , ascribed to the phonon-mediated screening which slightly opposes the Hubbard repulsion, is lost within an interval of a few tens of femtoseconds and can be understood as a fingerprint of electronic states largely decoupled from the lattice. Additionally, these results enforce the hypothesis, envisaged in the current literature, that the transient photoinduced states belong to a sort of *crossover phase* instead of an equilibrium metallic one.

DOI: [10.1103/PhysRevB.103.155120](https://doi.org/10.1103/PhysRevB.103.155120)

### I. INTRODUCTION

Disclosing the phase diagram of complex materials is pivotal for both fundamental material science and technology because of the high demand for a new generation of devices. Time-resolved spectroscopies have the chance to provide new insights on the physical processes responsible for switching collective phases as colossal magnetoresistance, high temperature superconductivity (HTSC), spin- and charge-density waves (SDW/CDW), as well as Mott insulating states [1,2]. Spectroscopies employing femtosecond (fs) laser pulses can capture the dynamics of many-body effects, as electron-electron correlations and/or strong electron-phonon coupling, responsible for driving band structure instabilities [3]. Among several experimental techniques, time- and angle-resolved photoemission spectroscopy (tr-ARPES) is an ideal tool to face this challenge since it can reveal the dynamics of the single-particle spectral function at ultrafast timescales. Indeed, tr-ARPES recently paved the way towards a deeper understanding of the Mott and Peierls instabilities affecting complex materials, which are conjectured to subtly drive to HTSC, CDW, and other puzzling collective phases [4]. Notably, tr-ARPES experimental layouts combining coherent optical excitations and extreme ultraviolet (EUV) probes, produced via the nonlinear high-order harmonic generation processes (HHG), have the chance to disclose how the Mott and Peierls instabilities develop in the temporal ( $\simeq 100$  fs) and momentum (in the entire first Brillouin zone) domains. This approach aims to investigate the timescale where electronic many-body effects cannot be overlooked [5].

In this paper, we report on the ultrafast dynamics of the two-dimensional transition-metal dichalcogenide  $1T$ -TaS<sub>2</sub>, investigated by means of tr-ARPES. We used a near-infrared (NIR) optical laser pulse to initiate a transient photoinduced phase transition and an EUV probe pulse to snapshot the sample's band structure evolution near the  $\Gamma$  point. The probe pulses were produced via HHG in noble gas (Ar). The sample was kept at a temperature of 30 K. Indeed, the  $1T$ -TaS<sub>2</sub> low temperature phase is marked by a puzzling interplay between Mott-insulating and CDW states [6,7]. Our data reveal that the switch of the photoinduced phase is accompanied by a subtle response of the lower Hubbard band (LHB), which promptly reacts to the NIR pulse by shifting its binding energy towards a slightly larger value (by  $\simeq 50$  meV). Such a feature lasts for a time comparable to the optical pump pulse length ( $\simeq 35$  fs) and mirrors a transient change of the onsite Coulomb repulsion energy ( $U$ ). These data suggest that the correction to the bare value of  $U$ , arising from the phonon-mediated screening which slightly opposes to the electron-electron Hubbard repulsion, is lost for at least a few tens of fs. Such an observation can be understood as a fingerprint of electronic states largely decoupled from the lattice.

### II. SAMPLE

The high-temperature structure of the  $1T$ -TaS<sub>2</sub> is sketched in Fig. 1(a). Specifically, it exhibits a trigonal crystal system consisting of S-Ta-S layers. The Mottness and the CDW phase are commonly ascribed to interlayers bonding effects, electron-electron correlations, and strong

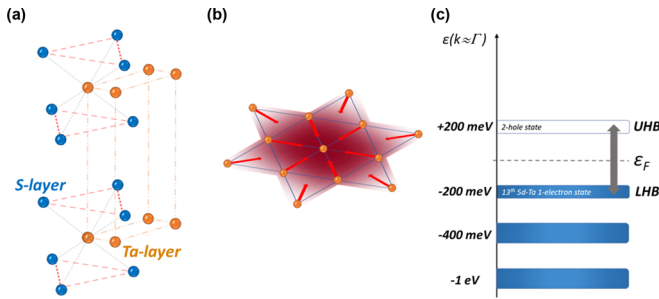


FIG. 1. Sketches of: (a) the  $1T$ -TaS<sub>2</sub> high-temperature undistorted octahedral structure; (b) the *David-star* cluster accompanying the c-CDW phase; (c) the  $1T$ -TaS<sub>2</sub> low-temperature band structure near the  $\Gamma$  point. LHB and UHB identify the lower and the upper Hubbard bands, respectively. The gray arrow marks the  $\simeq 400$  meV energy splitting, while the dashed gray line identifies the Fermi level ( $\epsilon_F$ ).

electron-phonon coupling [8,9]. Indeed, while at a temperature exceeding 542 K the  $1T$ -TaS<sub>2</sub> is metallic and exhibits an undistorted octahedral coordination, once cooled down to this (first) critical temperature it moves into a structural distorted state. Specifically, it develops an incommensurate charge-density wave phase (i-CDW). The latter approaches a perfect commensurate (c-CDW) state only below the (second) critical temperature of 180 K, marked by a rich phononic spectrum dominated by the (amplitude) mode centered at  $\simeq 2.4$  THz [10,11]. The c-CDW phase is accompanied by the appearance of *David-star* clusters made of 13 Ta atoms, each of them holding a  $d^1$  valence state [see Fig. 1(b)]. Near the  $\Gamma$  point the electrons are rearranged into three different  $5d$  bands, two of them filled and the third one partially occupied by the 13th (spare) electron. Such a feature is localized at a binding energy of  $\simeq -200$  meV and identified to be the LHB [6]. Therefore, a gap in the range of  $\simeq 200$  meV marks the Mott-insulating state, with an energy splitting between the LHB and its specular conduction band, i.e., the upper Hubbard band (UHB), of  $\simeq 400$  meV [see Fig. 1(c)]. The  $1T$ -TaS<sub>2</sub> phase diagram was extensively studied via equilibrium spectroscopies, but only thanks to the advent of table-top coherent light sources was it possible to disclose photoinduced phases and novel *hidden* states of matter [12,13]. Tr-ARPES experiments report an upper limit for the switch of the photoinduced phase in the order of less than  $\simeq 100$  fs. Moreover, the exact processes involved in the excitation of the electronic Mott states and the subsequent emergence of the CDW phase are still matter of intense research [12,14]. Furthermore, it is envisaged in the current literature that the transient photoinduced state of  $1T$ -TaS<sub>2</sub> cannot be exactly compared to the equilibrium metallic one but rather belongs to a sort of *crossover phase*. It is marked by signatures amenable to both the high (metallic) and low (insulating) temperature phases [7,15]. Our study concentrated on these open issues.

### III. EXPERIMENTAL LAYOUT

The experiment was performed at the CITIUS light source [16]. CITIUS is equipped with a Ti:Sapphire laser source

(Legend Elite Duo from *Coherent Inc.*) operating at a repetition rate of 5 KHz and delivering NIR pulses characterized by a central wavelength of 805 nm and a temporal duration of  $\simeq 35$  fs. A large portion of this NIR beam is used to seed a HHG source, designed to deliver a frequency comb covering photon energies between  $\simeq 12$  eV and  $\simeq 70$  eV [17]. This comb propagates up to an off-plane geometry monochromator holding a multiple EUV gratings selection. It is purposely designed to both efficiently diffract a single harmonic order and to limit the temporal stretching experienced by the EUV pulse, i.e., to keep the overall temporal resolution uniquely limited by the NIR pulse length [16,18]. For our purposes, the monochromator was operating a grating with 400 grooves/mm to efficiently diffract probe pulses centered at a photon energy of 21.6 eV, i.e., the 13th harmonic of the fundamental NIR emission. The exit slit was kept closed enough to guarantee a bandwidth of  $\simeq 100$  meV and a temporal resolution of  $\simeq 30$  fs. The EUV probe and the NIR pump were refocused in the tr-ARPES chamber by means of an Au-coated toroidal mirror ( $f = 1200$  mm) and an optical lens ( $f = 1500$  mm), respectively. The tr-ARPES chamber is equipped with a 5-axis manipulator, a liquid He closed circuit cryostat designed to cool samples down to 11 K, and an hemispherical analyzer (*R3000* from *VG Scientia*) characterized by an intrinsic energy resolution in the range of  $\simeq 20$  meV [16]. The  $1T$ -TaS<sub>2</sub> samples, provided by *HQ graphene*, were cleaved *in situ* in ultrahigh vacuum conditions (less than  $5 \times 10^{-10}$  mbar). X-rays photoemission spectroscopies (XPS) and band structure reconstruction, between the  $\Gamma$  point and the  $M$  one, were performed to both check the samples stoichiometric goodness and the correct exfoliation procedure. The optical pump fluence was set at a value of  $\simeq 2.5$  mJ/cm<sup>2</sup>, corresponding to NIR pulses carrying an energy of  $\simeq 1.6$   $\mu$ J (per pulse) focused on a  $\simeq 300$  (FWHM)  $\mu$ m spot.

### IV. RESULTS AND DISCUSSION

The time trace of Fig. 2(a) refers to the  $1T$ -TaS<sub>2</sub> band structure evolution, captured (near the  $\Gamma$  point) as a function of the pump-probe delay ( $\Delta t$ ). The main feature, localized at a binding energy ( $E_{LHB}$ ) of  $\simeq -200$  meV, is identified to be the LHB.  $E_{LHB}$  is defined to be the distance between the maximum spectral weight ( $SW$ ) and the Fermi level ( $\epsilon_F$ ). The time trace is built by integrating the tr-ARPES signal in the (momentum) domain between  $-0.3 \text{ \AA}^{-1}$  and  $+0.3 \text{ \AA}^{-1}$  and by removing a constant background from every energy-distribution curve (EDC) to highlight the spectral features nearby  $\epsilon_F$ . At a first look, the time trace is characterized by a prompt  $SW$  transfer across  $\epsilon_F$ , occurring at the coincident arrival time of the NIR pulse and the EUV probe ( $\Delta t = 0$  fs) and marking the  $1T$ -TaS<sub>2</sub> photoinduced phase. The Mott-Hubbard phase is recovered within a few hundreds of fs and further accompanied by a pronounced  $E_{LHB}$  modulation, matching the c-CDW amplitude ( $A_{lg}^{(2)}$ ) mode and mimicking the coherent structural distortion [10,19]. These collective oscillations last for a few tens of picoseconds and are further damped via phonon-phonon scattering processes [7,15].

Figure 2(b) presents the early range of the EDCs dynamics, captured between  $\Delta t = -25$  fs and  $\Delta t = +100$  fs, in steps of

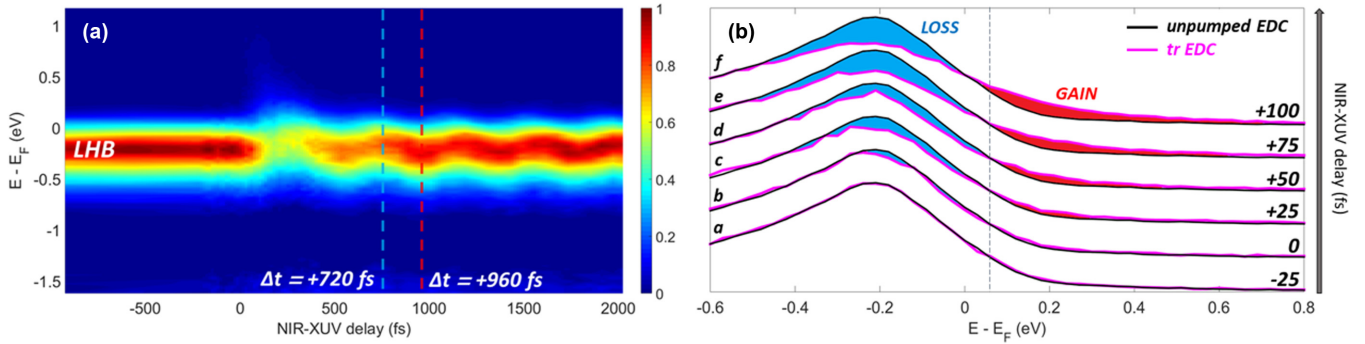


FIG. 2. (a) False colors representation of the LHB evolution as a function of the pump-probe delay,  $\Delta t$ . These data are the result of an interpolation process (for aesthetic reason only). We stress that the entire analysis is performed on raw data. The two vertical dashed lines mark the positions of the EDCs presented in Fig. 3. (b) Early range of the EDCs dynamics acquired between  $\Delta t = -25$  fs and  $\Delta t = +100$  fs, in steps of 25 fs. The violet lines refer to pumped EDCs, while the black one is the unpumped one. The blue areas mark the SW loss, while the red ones refer to the SW gain.

25 fs. Each snapshot compares the pumped EDC (violet trace) to the unpumped one (black trace). The EDCs at  $\Delta t = -25$  fs (a) exhibit qualitative identical traces, since the  $1T$ -TaS<sub>2</sub> still lies into an equilibrium state. Instead, at  $\Delta t = 0$  fs (b) there is a first evidence for SW loss in proximity of the LHB maximum (blue area) accompanied by a subsequent SW gain above  $\epsilon_F$  (red area). This suggests that the SW is transferred from the LHB across  $\epsilon_F$  on a timescale faster than our temporal resolution, resulting into a prompt filling of the Mott gap (above  $\epsilon_F$ ). This is consistent to the current literature [15,20]. Even more interesting are the EDCs acquired at  $\Delta t = +25$  fs and  $\Delta t = +50$  fs [(c)/(d)]. Indeed, while in the first one we reveal a growth in terms of SW loss (c), in the second snapshot it remains approximately constant (d). Only at  $\Delta t = +75$  fs (e) it is possible to find out a recovery in terms of SW loss, which further drastically increases (f) at larger ( $\Delta t = +100$  fs) delays [10]. Therefore, we reveal a timescale marked by a SW loss initiated by the coherent optical excitation, which continuously grows up to  $\Delta t = +50$  fs. Afterwards, the SW loss remains approximately constant for a few more tens of fs, until after at  $\Delta t \geq +75$  fs it progressively increases back, mimicking the coherent structural distortion. At this timescale we can expect that the electrons start to recouple to the lattice. The spectra in Fig. 3 offer a viewpoint on the coupling existing

between the electronic states and the lattice. The black line refers to the unpumped EDC ( $\Delta t \ll 0$  fs), while the blue and the red ones correspond to  $\Delta t = +720$  fs and  $\Delta t = +960$  fs, respectively. These EDCs match a c-CDW phonon phase difference of  $\simeq \pi$ , so between a maximum and a minimum of the  $E_{LHB}$  modulation, corresponding to an average peak shift of  $\simeq 130$  meV.

By integrating and normalizing the tr-ARPES signal in the (binding energies) domain between  $-100$  meV and  $-300$  meV [see Fig. 4(a)] we get the LHB differential intensity time trace,  $\Delta I_{LHB}(t)$ . Specifically, it is the result of normalizing each time trace value to the equilibrium one (average of the data at negative time delays). The normalized array minus one gives the absolute differential signal. Its behavior is fitted by means of the function:

$$f(t) = e^{-\frac{t^2}{2\tau_p^2}} \otimes (Ae^{-\frac{t}{\tau_1}} + Be^{-\frac{t}{\tau_2}} \sin(\Omega t + \phi)). \quad (1)$$

It follows from the convolution between a gaussian distribution, modeling how  $\Delta I_{LHB}(t)$  responds to the NIR pulse, and a relaxation function carrying the information on the recovering time of the Mott-Hubbard phase ( $\tau_1$ ), the lattice relaxation time ( $\tau_2$ ), as well as the magnitude ( $B$ ) and the frequency ( $\Omega$ ) of the c-CDW amplitude mode, accompanied by an extra phase term ( $\phi$ ). The fitting parameters give a maximum depletion of 32%, a recovering time of  $\tau_1 = 587.5 \pm 30.4$  fs, an amplitude and a frequency for the lattice structural response of  $B = 64.1 \pm 0.8$  meV and  $\Omega = 2.39 \pm 0.04$  THz, respectively, plus an extra phase of  $\phi = 4.8 \pm 0.3$  rad. The electrons populating the LHB are promoted into conduction bands localized (far) above  $\epsilon_F$ , at binding energies larger than  $+1$  eV, due to the photon energy of our optical excitation (1.54 eV). The transition between the LHB and the UHB is suppressed since our experimental layout is not designed to resonantly excite it. The UHB is so populated by electrons initially located at binding energies  $\simeq -1.3$  eV (S bands).

In addition to  $\Delta I_{LHB}(t)$ , we get the differential intensity of the background excitation continuum,  $\Delta I_{bg}(t)$ . It is built by integrating and normalizing the tr-ARPES signal in the (binding energies) domain between  $+400$  meV and  $+1.2$  eV [see Fig. 4(b)]. Its relaxation decay time provides the knowledge on the timescale of the electron-electron scattering in the

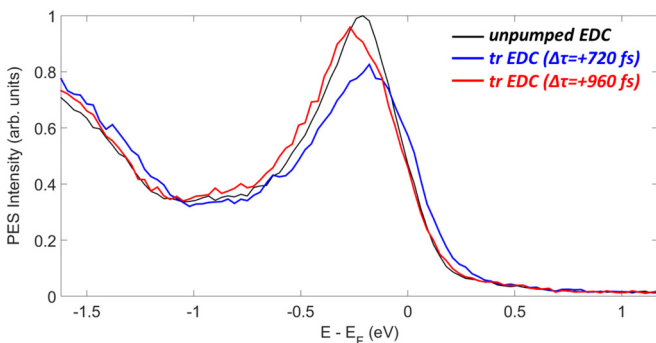


FIG. 3. Comparison between the unpumped (black line) and the pumped EDCs, captured at  $\Delta t = +720$  fs (blue line) and  $\Delta t = +960$  fs (red line).

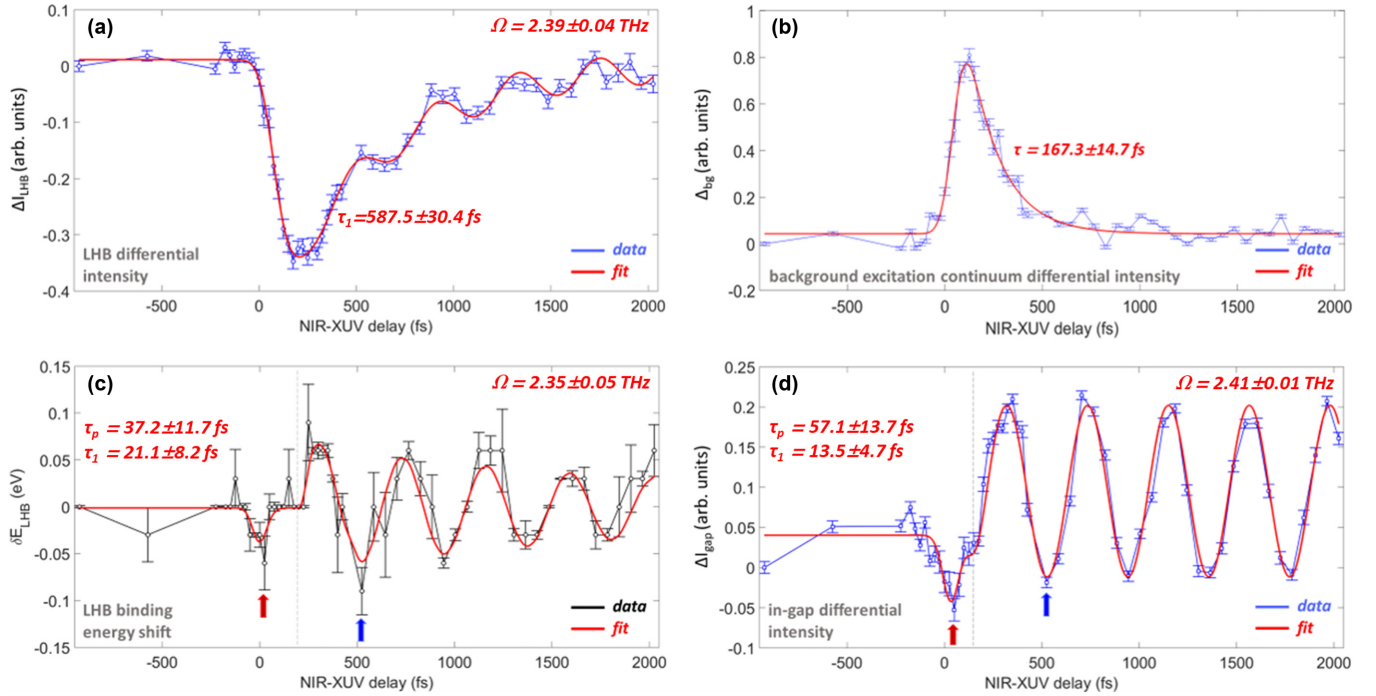


FIG. 4. (a) Differential LHB intensity time trace (blue dots),  $\Delta I_{\text{LHB}}(t)$ . (b) Differential background (bg) excitation continuum time trace (blue dots),  $\Delta I_{\text{bg}}(t)$ . (c) Binding-energy shift time trace (black dots),  $\delta E_{\text{LHB}}(t)$ . (d) Differential intensity integrated into a gap portion (blue dots),  $\Delta I_{\text{gap}}(t)$ . The red arrows are guides for the eyes to mark the prompt responses, while the blue ones indicate the first in-phase crests. The red lines refer to the fit functions.

continuum and increases as the energy approaches  $\epsilon_F$ . In our case we set the lower integration limit at +400 meV instead of  $\epsilon_F$  since at low energies the electronic response is largely entangled with the coherent structural dynamics. Indeed, the contribution nearby  $\epsilon_F$  could introduce a systematic overestimation of the overall relaxation decay time. Specifically,  $\Delta I_{\text{bg}}(t)$  is fitted by an exponential decay function, which gives a relaxation decay time equal to  $\tau = 167.3 \pm 14.6$  fs. Nonetheless, we stress that this value is only a (lower) limit for the overall relaxation decay time of the background continuum. The electron-electron scattering in the continuum (nearby  $\epsilon_F$ ), that we do not consider for the reason mentioned above, should increase the overall relaxation decay time, as reported in the current literature [20]. Estimating this value is fundamental to detach the timescale of the electron-electron scattering processes taking place in the continuum from the response involving correlated electronic Mott states.

The dynamics of the LHB energy shift,  $\delta E_{\text{LHB}}(t)$ , built by extrapolating the binding energy positions corresponding to each EDCs maximum, is shown in Fig. 4(c). Instead, the time trace in Fig. 4(d) refers to the differential gap intensity  $\Delta I_{\text{gap}}(t)$  obtained by integrating the tr-ARPES signal in the (binding energies) domain enclosed between  $-100$  meV and  $+100$  meV. Both  $\delta E_{\text{LHB}}(t)$  and  $\Delta I_{\text{gap}}(t)$  exhibit a similar qualitative behavior since they promptly react to the NIR pulse and reveal features within the first tens of fs. Indeed,  $\delta E_{\text{LHB}}(t)$  is marked by a prompt shift towards slightly higher (in magnitude) binding energies, and  $\Delta I_{\text{gap}}(t)$  exhibits a negative prompt signal (red arrows in Figs. 4(c) and 4(d)). These features are both accompanied by a fast recovery and a (almost) rigid oscillatory movement dominating the longer timescale.

These are fitted by means of the function:

$$s(t) = Ae^{-\frac{t^2}{2\tau_p^2}} \otimes e^{-\frac{t}{\tau_1}} + \theta(t - t_{ph})B \sin(\Omega t + \phi). \quad (2)$$

It follows from the convolution between a gaussian distribution, modeling how they promptly respond to the NIR pulse, and an exponential relaxation function, accounting for any electronic dynamics taking place in the first tens of fs. Instead, a sinusoidal function is used to reproduce the c-CDW response at the longer timescale. Since the c-CDW mode appears (at time  $t_{ph}$ ) only at the end of the electronic response decay, it is formally implemented by means of the product between the sinusoidal function and the Heaviside one,  $\theta(t - t_{ph})$ .

For  $\delta E_{\text{LHB}}(t)$ , the fitting parameters give us an electronic response ( $\tau_p$ ) of  $37.2 \pm 11.7$  fs, a decay ( $\tau_1$ ) of  $21.1 \pm 8.2$  fs, as well as a main frequency ( $\Omega$ ) of  $2.35 \pm 0.05$  THz and an extra phase ( $\phi$ ) of  $-0.3 \pm 0.1$  rad. The prompt shift is  $-36 \pm 4$  meV ( $A$ ), the modulation amplitude is  $41 \pm 5$  meV ( $B$ ), and the c-CDW starting time ( $t_{ph}$ ) is  $185.2 \pm 24.4$  fs. This means that the amount of binding energy shift is so in the range of few tens of meV, i.e., approximately one order of magnitude less than  $U$ , estimated to be  $\simeq 400$  meV [20,21]. Instead for  $\Delta I_{\text{gap}}(t)$ , the electronic response ( $\tau_p$ ) is  $57.1 \pm 13.7$  fs, the decay ( $\tau_1$ ) is  $13.5 \pm 4.7$  fs, the main frequency ( $\Omega$ ) is equal to  $2.41 \pm 0.01$  THz, and the extra phase ( $\phi$ ) is  $-0.4 \pm 0.2$  rad. In this case, the shift is  $-94 \pm 8$  meV ( $A$ ), the modulation amplitude is  $96 \pm 5$  meV ( $B$ ), and the starting time ( $t_{ph}$ ) is  $187.4 \pm 19.2$  fs. The main fitting parameters (responses, decays, and the main frequencies) are displayed in Figs. 4(c) and 4(d), too.

Since  $\delta E_{\text{LHB}}(t)$  and  $\Delta I_{\text{gap}}(t)$  exhibit similar responses at the fastest timescale ( $\Delta t \lesssim 100$  fs), these features, marked by the red arrow in Fig. 4(c) and 4(d) (as guide for the eyes), may be ascribed to the same class of physical processes involving electronic many-body effects. The gray vertical dashed lines are guides for the eyes to mark the positions of  $t_{ph}$ . However, the proof that these features cannot be driven by any structural response can be inferred from the following observation. Indeed, the first in-phase crest, marked by the blue arrow in Figs. 4(c) and 4(d) (as guide for the eyes), appears at a time-delay longer ( $\Delta t \simeq 500$  fs) than the intrinsic coherence period of the  $A_{1g}^{(2)}$  phonon ( $\simeq 420$  fs). Different phonon modes as the  $A_{1g}^{(1)}$  ( $\simeq 2.15$  THz) and  $E_g^{(1)}$  ( $\simeq 1.6$  THz) cannot contribute, too. Indeed, their intrinsic coherence periods are shorter ( $\simeq 460$  fs) or longer ( $\simeq 620$  fs) than the first in-phase crest position [10,19].

We propose the following phenomenological scenario to explain the  $\delta E_{\text{LHB}}(t)$  prompt response. Physical systems developing Mott-insulating phases exhibit a localization of the half-filled band at a binding energy equal to  $-U/2$  accompanied by a gap opening at  $\epsilon_F$ , where  $U$  is the (bare) Coulomb repulsion energy [2]. It was pointed out by several authors that the Mott-Hubbard scenario is incomplete to model complex materials marked by electronic Mott states strongly coupled to the lattice [22]. Precisely,  $U$  is predicted to be (partially) reduced by the strong electron-phonon coupling itself, since the phonons mediate a retarded attractive density-density interaction, which slightly opposes to the electron-electron mutual repulsion, i.e., the phonons partially screen the Hubbard interaction [23,24]. The arrival of a coherent optical excitation triggers the delocalization of electrons initially located at valence states, corresponding to a prompt gain of carriers above  $\epsilon_F$  and a subsequent lack of electronic Mott states. This implies a transient loss of the charge density required to sustain the phonon-mediated screening. It lasts for a temporal interval comparable to the optical pump pulse length. Formally, the coupling between the electrons and the lattice leads to the reduction of the onsite Coulomb repulsion energy  $U$  towards an effective (dressed) value equal to  $U - g^2/\omega$ , where  $\omega$  and  $g$  are the intrinsic frequency of the boson field and the coupling constant, respectively [22]. The laser field triggers a dipole moment, which modifies  $\tilde{U}$  into a time-dependent variable:

$$\tilde{U} \rightarrow \tilde{U}(t) = U - \frac{g^2}{\omega} + |e| \frac{g}{\omega} p(t), \quad (3)$$

where  $e$  and  $p(t)$  are the electric charge and the pulse (gaussian) profile, respectively [25,26]. Figure 5 offers a sketch for the proposed scenario, where the black line refers to the  $E_{\text{LHB}}$  dynamics, i.e.,  $-\tilde{U}(t)/2$ . At the arrival of the optical pump pulse,  $E_{\text{LHB}}$  promptly moves towards its bare value, identified by the gray (dashed) line, profiling the pulse rising edge. The blue shadow area marks the prompt loss of charge density. At longer timescale it follows the expected coherent structural distortion. Such a response is qualitatively reproduced by means of the function  $s(t)$ .

The  $\delta E_{\text{LHB}}(t)$  prompt response [see Fig. 4(c)], combined to the early range of the EDCs dynamics [see Fig. 2(b)], suggest that the electronic Mott states are practically decoupled from the lattice up to  $\Delta t \simeq +50$  fs. Indeed, the fact that the  $SW$

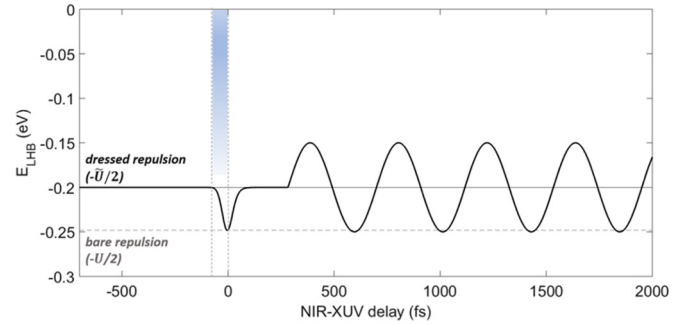


FIG. 5. Dynamics of the dressed Hubbard repulsion at the arrival of the NIR laser pulse (black full line). The grey dashed line refers to the bare value, while the blue dashed area is a guide for the eye marking the prompt charge delocalization (loss).

loss promptly increases for a temporal interval comparable to the optical pump pulse length, identifies the timescale where the Mott and CDW dynamics are dissected. Additionally, the simultaneous LHB binding energy shift explained in terms of a prompt loss of phonon mediated screening opposing to the Hubbard repulsion energy, supports this hypothesis.

Moreover, we stress that the exact electronic processes cannot be properly resolved in our experiment, since this would require to push the temporal resolution towards the few fs timescale. This means to design a tr-ARPES layout combining few-cycles optical pulses and EUV probes characterized by a larger bandwidth. Nonetheless, this approach embeds an intrinsic disadvantage due to the pulse time-bandwidth product. Indeed, increasing the temporal resolution implies a reduction of the experimental energy resolution [5]. We suggest that the proper choice is to look for a sort of balanced temporal and energy resolutions. We are confident that this experimental layout will be able to properly disclose the involved electronic processes and consequently to give a robust quantitative estimation for  $g$  and  $\omega$ , which define the correction to  $U$ , too.

To qualitatively support and strength this scenario, it is necessary to discuss and rule out the competing processes that could give birth to these features, too. First, we underline that the  $\delta E_{\text{LHB}}(t)$  prompt response cannot be ascribed to any chemical potential shift driven by nonthermal electronic excitations. Indeed, Fig. 2(b) reports the early range of the EDCs dynamics, and in the interval between  $\Delta t = -25$  fs and  $\Delta t = +50$  fs it does not move (see the vertical dashed line as a guide for the eye) and remains approximately constant. Only at  $\Delta t \gtrsim +75$  fs it is possible to reveal a significant chemical potential displacement, which mimics the coherent lattice structural dynamics. These data suggest that the coherent optical excitation does not affect the chemical potential at a timescale dominated by the electron-electron correlations. Secondary, it was recently proposed that the insulating phase of  $1T$ -TaS<sub>2</sub> should mainly be the result of orbital texturing effects, rather than a Mott transition [27]. If this is the case, the fastest dynamics in the photoinduced phase should be set by the electron-electron scattering processes in the continuum, as expected in systems characterized by orbitally orders. Nevertheless, we clearly see that the background excitation continuum has a relaxation decay time slower ( $\tau = 167.3 \pm 14.6$  fs) than the observed prompt responses. This

means that the electron-electron correlations cannot be overlooked and the  $1T$ -TaS<sub>2</sub> insulating phase can be mainly pictured in terms of the Mott-Hubbard model [28,29]. We stress that orbital texturing effects may have some role in the building-up of the  $1T$ -TaS<sub>2</sub> phase diagram, which goes beyond the goal of this work. Recent tr-ARPES experiments and dynamical mean field theory (DMFT) results, pointed out how coherent optical excitations may not drive  $1T$ -TaS<sub>2</sub> into a metallic state qualitatively similar to the high-temperature equilibrium one but rather into a *crossover phase* [30–35]. The latter is marked by both an electron temperature comparable to the equilibrium metallic state one and a ratio between the effective Coulomb repulsion energy and the Hubbard bandwidth ( $W$ ) qualitatively similar to the Mott-Hubbard phase one. These are the features amenable to both the high temperature (metallic) and the low temperature (insulating) phases [7,15]. Our experimental findings offer qualitative insights on the features marking the photoinduced phase and consequently a viewpoint on the mentioned *crossover phase*.

## V. CONCLUSIONS

Summarizing, we presented results on the ultrafast dynamics of the two-dimensional transition-metal dichalcogenide  $1T$ -TaS<sub>2</sub>. We used NIR laser pulse to initiate a photoinduced phase transition in  $1T$ -TaS<sub>2</sub> and an EUV probe to snapshot the sample's band structure evolution near the  $\Gamma$  point. Our study mainly concentrated on the dynamics taking place in the first 100 fs. Our data reveal that the  $SW$  is promptly transferred from the LHB towards the conduction bands, resulting into a filling of the Mott-gap states (above  $\epsilon_F$ ). The  $SW$  loss grows for a time comparable to the NIR pump pulse length, and later stays approximately constant for few more tens of fs. Within

this temporal interval there is no evidence for a chemical potential shift, too. Just at  $\Delta t \geq +75$  fs the  $SW$  loss grows again, further mimicking the coherent structural distortion at longer timescales. Simultaneously, the LHB promptly reacts to the coherent optical excitation by shifting its binding energy towards a slightly larger value. Such a feature lasts for a time comparable to the optical pump pulse length and mirrors a transient change of the Coulomb repulsion energy. We proposed the following phenomenological scenario to explain it. At equilibrium, the Hubbard repulsion is slightly weaker than its bare value. This is a consequence of the strong electron-phonon coupling, i.e., the phonons mediate a retarded attractive density-density interaction, which slightly screens and opposes to  $U$ . To our knowledge, such a feature has never been observed up to now, although theoretically predicted. The loss of phonon-mediated screening, consequently to the arrival of the optical pump pulse, can explain the transient LHB binding energy shift. We stress that disclosing the electronic processes responsible for switching these prompt processes (up to  $\Delta t \simeq +50$  fs) require to push the temporal resolution towards the few-fs timescale. We suggest that the proper choice is to look for a balanced amount of temporal and energy resolutions. This currently goes beyond the scope of our work. However, we are confident that our results may pave the way to future and deeper investigations on the dynamics of several complex materials (not only dichalcogenide as  $1T$ -TaS<sub>2</sub>) marked by puzzling collective phases.

## ACKNOWLEDGMENTS

This work has received funding from the European Union's Horizon 2020 research and innovation programme under Grant Agreement No. 654360 NFFA-Europe.

- 
- [1] J. Orenstein, Ultrafast spectroscopy of quantum materials, *Phys. Today* **65**(9), 44 (2012).
- [2] C. Giannetti, M. Capone, D. Fausti, M. Fabrizio, F. Parmigiani, D. Mihailovic, Ultrafast optical spectroscopy of strongly correlated materials and high-temperature superconductors: A non equilibrium approach, *Adv. Phys.* **65**, 58 (2016).
- [3] M. Buzzi, M. Foerst, R. Mankowsky, and A. Cavalleri, Probing dynamics in quantum materials with femtosecond X-rays, *Nat. Rev. Materials* **3**, 299 (2018).
- [4] R. Comin and A. Damascelli, ARPES: A probe for electronic correlations, *Strongly Correlated Systems* (Springer, Berlin, Heidelberg, 2015), pp. 31–71.
- [5] S. Y. Kruchinin, F. Krausz, and V. Yakolev, Strong-field phenomena in periodic systems, *Rev. Mod. Phys.* **90**, 021002 (2018).
- [6] K. Rossnagel, On the origin of charge-density waves in select transition-metal dichalcogenides, *J. Phys. Condens. Matter* **23**, 213001 (2011).
- [7] L. Perfetti, P. A. Loukakos, M. Lisowski, U. Bovensiepen, M. Wolf, H. Berger, S. Biermann, and A. Georges, Femtosecond dynamics of electronic states in the Mott insulator  $1T$ -TaS<sub>2</sub> by time resolved photoemission spectroscopy, *New J. Phys.* **10**, 053019 (2008).
- [8] E. Tosatti and P. Fazekas, On the nature of the low-temperature phase of  $1T$ -TaS<sub>2</sub>, *J. Phys.* **37**, 165 (1976).
- [9] K. Rossnagel and N. V. Smith, Spin-orbit coupling in the band structure of reconstructed  $1T$ -TaS<sub>2</sub>, *Phys. Rev. B* **73**, 073106 (2006).
- [10] L. V. Gasparov, K. G. Brown, A. C. Wint, D. B. Tanner, H. Berger, G. Margaritondo, R. Gaál, and L. Forró, Phonon anomaly at the charge ordering transition in  $1T$ -TaS<sub>2</sub>, *Phys. Rev. B* **66**, 094301 (2002).
- [11] G. Gruener, *Density Waves in Solids*, Frontiers in Physics (CRC Press, 1994).
- [12] J. C. Petersen, S. Kaiser, N. Dean, A. Simoncig, H. Y. Liu, A. L. Cavalieri, C. Cacho, I. C. E. Turcu, E. Springate, F. Frassetto, L. Poletto, S. S. Dhesi, H. Berger, and A. Cavalleri, Clocking the Melting Transition of Charge and lattice Order in  $1T$ -TaS<sub>2</sub> with Ultrafast Extreme-ultraviolet Angle-resolved Photoemission Spectroscopy, *Phys. Rev. Lett.* **107**, 177402 (2011).
- [13] L. Stojchevska, I. Vaskivskiy, T. Mertelj, P. Kusar, D. Svetin, S. Brazovskii, and D. Mihailovic, Ultrafast switching to a stable

- hidden quantum state in an electronic crystal, *Science* **344**, 177 (2014).
- [14] I. Avigo, I. Vaskivskiy, M. Ligges, M. Kallaene, K. Rossnagel, L. Stojchevska, D. Mihailović, and U. Bovensiepen, *Accessing and probing of the photo-induced hidden state in 1T-TaS<sub>2</sub> with time- and angle-resolved photoemission spectroscopy*, SPIE Proceedings 9931, Spintronics IX, 99313V (SPIE, 2016).
- [15] L. Perfetti, P. A. Loukakos, M. Lisowski, U. Bovensiepen, H. Berger, S. Biermann, P. S. Cornaglia, A. Georges, and M. Wolf, Time Evolution of the Electronic Structure of 1T-TaS<sub>2</sub> through the Insulator-Metal Transition, *Phys. Rev. Lett.* **97**, 067402 (2006).
- [16] C. Grazioli, C. Callegari, A. Ciavardini, M. Coreno, F. Frassetto, D. Gauthier, D. Golob, R. Ivanov, A. Kivimäki, B. Mahieu, B. Bučar, M. Merhar, P. Miotti, L. Poletto, E. Polo, B. Ressel, C. Spezzani, and G. De Ninno, CITIUS: An infrared-extreme ultraviolet light source for fundamental and applied ultrafast science, *Rev. Sci. Instrum.* **85**, 023104 (2014).
- [17] T. Pfeiffer, C. Spielmann, and G. Gerber, Femtosecond x-ray science, *Rep. Prog. Phys.* **69**, 443 (2006).
- [18] L. Poletto and F. Frassetto, Time-preserving grating monochromators for ultrafast extreme-ultraviolet pulses, *Appl. Opt.* **49**, 5465 (2010).
- [19] O. R. Albertini, R. Zhao, R. L. McCann, S. Feng, M. Terrones, J. K. Freericks, J. A. Robinson, and A. Y. Liu, Zone-center phonons of bulk, few-layer, and monolayer 1T-TaS<sub>2</sub>: Detection of commensurate charge density wave phase through Raman scattering, *Phys. Rev. B* **93**, 214109 (2016).
- [20] M. Ligges, I. Avigo, D. Golež, H. U. R. Strand, Y. Beyazit, K. Hanff, F. Diekmann, L. Stojchevska, M. Kalläne, P. Zhou, K. Rossnagel, M. Eckstein, P. Werner, and U. Bovensiepen, Ultrafast Doublon Dynamics in Photoexcited 1T-TaS<sub>2</sub>, *Phys. Rev. Lett.* **120**, 166401 (2018).
- [21] I. Avigo, F. Queisser, P. Zhou, M. Ligges, K. Rossnagel, R. Schützhold, and U. Bovensiepen, Doublon bottleneck in the ultrafast relaxation dynamics of hot electrons in 1T-TaS<sub>2</sub>, *Phys. Rev. Research* **2**, 022046(R) (2020).
- [22] J. E. Hirsch, Dynamic Hubbard Model, *Phys. Rev. Lett.* **87**, 206402 (2001).
- [23] G. Sangiovanni, M. Capone, C. Castellani, and M. Grilli, Electron-phonon Interaction Close to a Mott Transition, *Phys. Rev. Lett.* **94**, 026401 (2005).
- [24] D. Golez, M. Eckstein, and P. Werner, Dynamics of screening in photodoped Mott insulator, *Phys. Rev. B* **92**, 195123 (2015).
- [25] P. Werner and M. Eckstein, Effective doublon and hole temperature in the photo-doped dynamic Hubbard model, *Struct. Dyn.* **3**, 023603 (2016).
- [26] P. Werner and M. Eckstein, Field-induced polaron formation in the Holstein-Hubbard model, *Euro. Phys. Lett.* **109**, 37002 (2015).
- [27] T. Ritschel, J. Trinckauf, K. Koepf, B. Büchner, M. V. Zimmermann, H. Berger, Y. I. Joe, P. Abbamonte, and J. Geck, Orbital textures and charge density waves in transition metal dichalcogenides, *Nat. Phys.* **11**, 328 (2015).
- [28] S. Hellmann, T. Rohwer, M. Kalläne, K. Hanff, C. Sohr, A. Stange, A. Carr, M. M. Murnane, H. C. Kapteyn, L. Kipp, M. Bauer, and K. Rossnagel, Time-domain classification of charge-density wave insulators, *Nat. Commun.* **3**, 1069 (2012).
- [29] C. Sohr, A. Stange, M. Bauer, and K. Rossnagel, How fast a Peierls-Mott insulator can be melted?, *Faraday Discuss.* **171**, 243 (2014).
- [30] C. W. Chen, J. Choe, and E. Morosan, Charge density waves in strongly correlated electron systems, *Rep. Prog. Phys.* **79**, 084505 (2016).
- [31] J. A. Wilson, F. J. Di Salvo, and S. Mahajan, Charge-density waves and superlattices in metallic layered transition-metal dichalcogenides, *Adv. Phys.* **24**, 117 (1975).
- [32] T. Rohwer, S. Hellmann, M. Wiesenmayer, C. Sohr, A. Stange, B. Slomski, A. Carr, Y. Liu, L. M. Avila, M. Kallaene, S. Mathias, L. Kipp, K. Rossnagel, and M. Bauer, Collapse of long-range charge order tracked by time-resolved photoemission at high momenta, *Nature (London)* **471**, 490 (2011).
- [33] G. Sangiovanni, M. Capone, and C. Castellani, Relevance of phonon dynamics in strongly correlated systems coupled to phonons: dynamical mean-field theory analysis, *Phys. Rev. B* **73**, 165123 (2006).
- [34] S. Sayyad and M. Eckstein, Coexistence of excited polarons and metastable delocalized states in photoinduced metals, *Phys. Rev. B* **91**, 104301 (2015).
- [35] P. Werner and M. Casula, Dynamical screening in correlated electron systems—from lattice models to realistic materials, *J. Phys. Condens. Matter* **28**, 383001 (2016).